Composites: Part A xxx (2016) xxx–xxx

Contents lists available at ScienceDirect

Composites: Part A

journal homepage: www.elsevier.com/locate/compositesa

Friction of carbon fibre tows

Daniel M. Mulvihill *, Olga Smerdova [1], Michael P.F. Sutcliffe

Department of Engineering, University of Cambridge, Trumpington Street, Cambridge CB2 1PX, UK

ARTICLE INFO

Article history:
Received 22 May 2016
Received in revised form 21 August 2016
Accepted 29 August 2016
Available online xxxx

Keywords:
A. Carbon fibres
A. Tow
E. Forming
Friction

ABSTRACT

The fundamental frictional behaviour of carbon fibre tows relevant to composite fabric forming is explored. Tow-on-tool and tow-on-tow contact are considered. For tow-on-tool contact, an experiment is devised to simultaneously observe the true filament contact length and measure the friction force over a range of normal loads. Filament contact length is not constant, as would be given from an idealised assumption of parallel touching filaments, but increases in a characteristic manner with normal load. Friction force follows a power law variation with normal load with exponent in the range 0.7–1. Accounting for the evolving contact length in a Hertzian calculation of the real contact area produces a contact area versus load variation which differs only by a constant factor from the measured friction force curves. Thus, the results agree with a 'constant interface strength' model of friction. Tow orientation and sizing are found to have a significant effect on friction by altering the real contact area.

1. Introduction

Use of polymer composite materials is growing in the aerospace and automotive sectors [1,2], where there is an increasing need to produce complex parts in a cost-effective manner. Such parts can be produced by a variety of forming techniques from a wide range of dry or pre-impregnated fabrics. A fabric usually consists of a woven or stitched arrangement of fibre tows, while the tows themselves are in the form of a flattened yarn containing many thousands of individual continuous filaments. Thus a classification into three scales can be made: macro (fabric or ply level), meso (tow level) and micro (filament level). The deformations that occur across these scales during the forming process are critical in determining the structural and dimensional integrity of the final part. Depending on the required part shape and on the fabric type, undesirable structural features such as thickness changes, wrinkles or voids can occur at certain locations. A robust predictive modelling capability for the deformations is much in demand by the composites industry, but is yet to be realised as the physical mechanisms at play in fabric forming are not fully understood. An accurate description of the forces in the system is required to predict deformations. Apart from the normal forces imparted by the tool, friction is the other dominant force generating mechanism occurring. The type of contact is always either filament-filament or filament-tool, but this picture is somewhat complicated by the structural arrangement of the fabric (a particular frictional interaction can be classified as intra-tow, inter-tow, inter-ply, tow-tool and ply-tool). In this paper, our focus is on tow friction: inter-tow and between tow and tool. These cases would be particularly pertinent to the dry fabric pre-forming stage, prior to a subsequent resin infusion stage (for example: resin transfer moulding). However, results could also have application in other composite manufacturing processes including fabric manufacture or inter-ply shear of woven fabrics.

A good place to begin studying tow friction is with the considerable body of textile friction research carried out since the 1940s. Early work focused on polymer materials such as nylon [3,4], and natural materials like viscose rayon [3,5] and wool [6,7]. Useful summaries of the main developments in fibre friction are given in Rubenstein [8], Howell et al. [9] and Yuksekkaya [10]. Essentially, it emerged that fibrous materials (unlike most solids) do not usually conform to the direct proportionality between friction force F and normal force W given by Amonton's Law [11] (i.e. $F = fW$, where f is the coefficient of friction). Instead, a more general description was proposed [3] whereby $F = kW^n$ (k and n being experimentally determined constants). This more general description applied (with $n < 1$) equally to experiments carried out on individual fibre filaments [12–15] as it did to those on multi-filament arrangements [5,16] (and for both filament-filament [14] and filament-on-flat [15] type experiments).

The contact of flat metal surfaces generally obeys the direct proportionality in Amonton's Law (i.e. $n = 1$). Bowden and Tabor's

* Corresponding author presently at: School of Engineering, University of Glasgow, G12 8QQ, UK.
E-mail address: daniel.mulvihill@glasgow.ac.uk (D.M. Mulvihill).
[1] Present address: Institut Pprime, CNRS, ISAE-ENSMA, Université de Poitiers, F-86962 Futuroscope Chasseneuil, France.

http://dx.doi.org/10.1016/j.compositesa.2016.08.034
1359-835X/

'adhesion' theory [17] offers an explanation: namely, that surface bonding (or adhesion) occurs at the points of intimate contact and that the friction force is simply given by the shear strength τ of these junctions times the real contact area A (i.e. $F = \tau A$). Around the same time as Bowden and Tabor's work, it had been shown that the 'real contact area' was, in fact, directly proportional to the applied load W. The combination of these two relationships led directly to Amonton's Law. Therefore, it is the real contact area that determines the frictional behaviour. Nominally flat surfaces actually consist of a stochastic height distribution of small asperities. Bowden and Tabor realised that plastic deformation of these asperity junctions would explain the proportionality of real contact area with normal load although this did not explain why surfaces operating below the plastic limit also obeyed Amonton's Law. It was not until the contributions of Archard [18] and subsequently, Greenwood and Williamson [19], that an explanation allowing for elastic deformation was given. Due to Hertzian contact mechanics, elastic spheres in contact should generate a contact area which varies with $W^{2/3}$. However, Archard [18] and Greenwood and Williamson [19] realised that the overall real contact area would be directly proportional to normal load if new asperity contacts developed in such a way that the number of asperity contacts was proportional to the normal load. In this situation, the overall average contact area of an individual asperity contact remains constant with increasing load. Greenwood and Williamson [19] showed that this requirement was exactly satisfied for an exponential distribution of asperity heights and very closely approximated for the more representative Gaussian distribution. Essentially, with surfaces involving elastically deforming asperities, the development of new contact areas is required in order to push the exponent n from 2/3 towards unity. In fact, Barber [20] has recently shown that, as long as there is enough multiscale contact to a surface, Amonton's Law will be obeyed regardless of the particular friction law assumed at the finest scale, and that Archard and Greenwood and Williamson essentially both rely on the same multiscale nature of surfaces.

Contact involving fibrous materials also involves deformation of asperity contacts, but a key difference is the overall cylindrical nature of the filaments. Elastically deforming crossed cylinders give a contact area which varies with $W^{2/3}$ while parallel cylinders and cylinder-on-flat contacts give a variation with $W^{1/2}$. Therefore, the appearance of the power law relation is not surprising in filament contact. That n is greater than 2/3 in some studies on individual filament contact (crossed or parallel), may be explained by the same sort of effect modelled by Greenwood and Williamson for metals, of increasing numbers of local asperity contacts with increasing load, or by the existence of some plastic deformation [4]. However, the behaviour of a fibrous assembly of filament contacts is likely to have an entirely different response from that of an isotropic solid, so that asperity models used for metals [19,21] cannot be directly applied.

Much of the work discussed above has been on single filaments made from polymer or natural material and comparatively less work has been carried out on multi-filament arrangements or on carbon filaments. Two important studies on individual carbon filaments were carried out by Roselman and Tabor [14,15]. The first [14], was on the contact of two crossed filaments and this showed an area variation with $W^{2/3}$ in line with the elastic prediction. The second [15], was on the contact of a carbon filament and various rough steel surfaces. Here, the values of the load index n were much closer to unity than the $n = 1/2$ (smooth counterface) and $n = 2/3$ (rough counterface) values predicted by theory. One type of fibre gave values of n between 0.7 and 0.8, while the values for the other type were closer to unity. The authors did not have an unequivocal explanation for this, but noted that the softer carbon filaments tested gave values of n closer to unity and surmised that this could be caused by a flattening effect attributed to wear. Applying the adhesion concept of friction, they found the interfacial shear strength of the filaments against the steel to be of the order of 15–50 MPa. They also noted an increase in friction with decreasing surface roughness (particularly for smoother surfaces - a behaviour also found with tows in Mulvihill and Sutcliffe [22]).

We can expect the frictional behaviour of a tow to be more complicated than that of a single filament. A tow consists of thousands of filaments with a large number of filaments through the width and thickness. Some recent work has focused exclusively on tow friction [23–26]. Cornelissen et al. [23] developed a contact model for calculation of real contact area and friction for tows in contact with rough surfaces. The model assumes smooth filaments, but accounts for two scales of asperity sizes on the rough surface based on simple Hertzian contact mechanics for the larger asperities and a Greenwood-Williamson type approach for the finer asperities. Predicted values of the load index n were quite close to unity varying from 0.84 to 0.99. In line with experiment, the model predicts higher real contact area and friction for the smoother surfaces. As well as the questionable assumption that a tow fibre assembly behaves like an isotropic elastic solid (implicit in the asperity modelling), an additional important simplification in the model is the assumption that there is an idealised arrangement of parallel touching filaments in the tow contact zone. Cornelissen et al. [24] and Chakladar et al. [26] have conducted recent *experimental* investigations on tow friction. They found that: tow-on-tool friction appears to be higher for contact with a smooth surface than for a rough one [24], that tow-on-tow friction is about 2.5 times higher for the parallel than for the perpendicular arrangement [24,26], and that the friction was not affected much by the number of filaments in the tow [26] or by the tow sizing [24]. The value of the load index n was in the range 0.86–0.91 in Cornelissen et al. [24], and appears to have been even closer to unity in Chakladar et al. [26].

Recently, our group (Smerdova and Sutcliffe [27,28]) has developed a technique to observe the real filament contact length in contact between a smooth tool and carbon fibre fabric. The contact area is imaged via an optical microscope through a glass plate pressed against the fabric, with a semi-reflective coating on the glass of silica and chromium specially optimised to show only the filaments in contact. Although the focus of measurements was on fabric undergoing shearing, a notable result was that, contrary to the idealised filament contact assumption, the real contact length of filament was surprisingly small. At the test pressure of 2 kPa, the contact length within a tow was only 4–8% of the idealised contact length assuming perfectly parallel touching filaments [28]. In the current paper, we use the optical coating technique to probe this issue in more depth and determine the relationship between real filament contact length and normal load in tow-on-tool contact by pressing on tows over a wide range of normal pressures. At each normal load step, we simultaneously measure filament contact length and friction force. We determine the F–W curves and consider how they are affected by the contact length and contact area versus load behaviour. Finally, we explore the frictional behaviour of normally loaded tow-on-tow contacts. The effect of factors such as filament sizing are also examined and, in the case of tow-on-tow friction, tow orientation.

2. Experimental approach

2.1. Test procedure (tow-on-tool)

A new experimental rig has been developed for the investigation. A schematic side and plan view is given in Fig. 1 and a photograph of the rig is shown in Fig. 2. The key capabilities are the

Please cite this article in press as: Mulvihill DM et al. Friction of carbon fibre tows. Composites: Part A (2016), http://dx.doi.org/10.1016/j.compositesa.2016.08.034

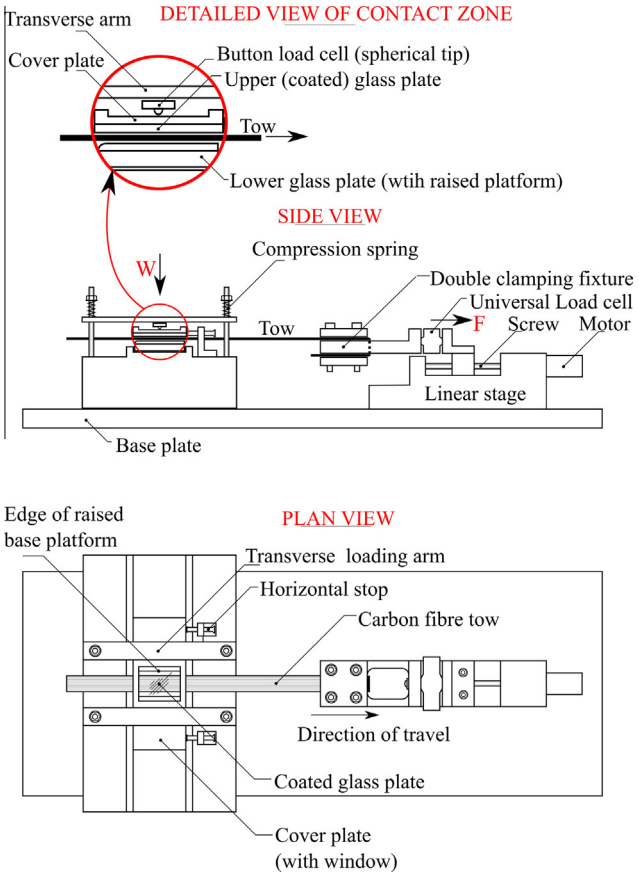

Fig. 1. Schematic drawing of experimental rig: detailed view of contact zone (top), side view (middle) and plan view (bottom). Setup shown here for tow-on-tool testing. (For interpretation of the references to colour in this figure legend, the reader is referred to the web version of this article.)

Fig. 2. Photograph of rig in-situ under optical microscope. (For interpretation of the references to colour in this figure legend, the reader is referred to the web version of this article.)

ability to apply accurate normal loads W to a carbon fibre tow, to allow imaging of the true length of carbon filament in contact L (for tow-on-tool contact) over a range of loads, and to concurrently measure the associated friction force F at each normal load step. The visualisation technique for imaging the filaments in contact relies on the technique developed by Smerdova and Sutcliffe [27] whereby a special semi-reflective coating alters the refractive properties of a glass plate so that only the filaments touching the plate are highlighted.

An appropriate length of tow (for use in the rig) was firstly cut from the roll of tow material. The two cuts were made across 'taped sections' (using masking tape) so as not to disturb the arrangement of filaments. Two additional taped regions were also created, at some distance from either side of the contact zone to help hold the tow together during the test. The tow was then clamped in the double clamping fixture shown in Fig. 1 and positioned to rest on a lower glass plate with a raised platform. An upper coated glass plate (fixed to an aluminium alloy cover plate) was then balanced on top of the tow with the coating touching the filaments. Additional load was then applied by screwing down on four compression springs so that the spherical tips of two button load cells (fixed to transverse arms) pressed onto the surface of the cover plate. These two points of load application are equidistant on either side of the tow so that applying equal loads (using the load cell readout) at each point ensures that the upper plate remains parallel with the lower plate. This system worked well for ensuring uniform loading of the tows. A range of normal loads could be applied up to the load capacity of the two load cells (22.2 N each).

At each normal load step, a representative section of the tow contact zone was imaged using a microscope. Thus, the experiment was carried out with the rig in-situ under the microscope as shown in Fig. 2. A window in the cover plate, as shown in Fig. 1, makes the contact zone (viewed through the coated glass plate) visible to the microscope. The resulting images clearly show the individual contacting filaments (Fig. 3). After scanning the contact zone, the friction force can also be measured at a given load step. This was done using a load cell attached to a screw-driven linear stage by pulling out the tow at constant speed (0.0066 mm/s) by a distance of 1 mm at each normal load increment. Most tests consisted of about 14 normal loading steps resulting in a total distance of travel of about 14 mm. A new tow specimen was not used for each normal load step as variability between sections of tow cut from the roll introduced variability into the F-W curve, thereby somewhat obscuring the underlying behaviour associated with increasing the normal load. Instead the entire test was done by 'pulling through' the same tow specimen. After each 1 mm pull-through, the stage was stopped and the procedure repeated by further increasing the normal load and scanning the contact zone. Two adjustable stops were positioned against the upper plate to prevent horizontal movement during tow pull-out and the edges of the glass plates on the incoming tow side were rounded to eliminate any edge effects on the friction force measurements. The nominal length of tow in contact was 23.75 mm.

Initially, a set of tests were carried out involving only normal loading (same portion of tow scanned each time). A second set of tests were then conducted (as described above) to include both normal loading and tangential pull-out to determine the friction force (here the scanned portion of tow changes gradually as the test proceeds). Each test was repeated five times with a new tow specimen to give an indication of repeatability.

2.2. Materials and equipment

Two types of carbon fibre tow were tested: T700SC-12k-60E and T700SC-12k-50C (Toray Industries, Tokyo, Japan) [29].

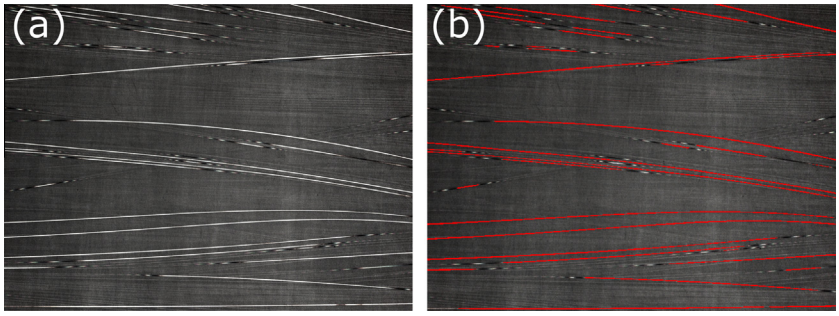

Fig. 3. (a) Example raw image from microscope camera and (b) post-processed image showing detected contacting filaments (in red). Image size: 1183.82 μm × 887.86 μm (magnification: ×10). (For interpretation of the references to colour in this figure legend, the reader is referred to the web version of this article.)

'T700S' denotes the fibre type (tensile strength of 4.9 GPa), 'C' denotes that the fibres were never twisted, 12k indicates that both tows have approximately 12,000 filaments, '6' and '5' denote the sizing type ('6' denotes compatibility with epoxy, while '5' denotes a more general compatibility with epoxy, phenolic, polyester, and vinyl-ester systems). The letters 'E' and 'C' denote the amount of sizing in weight percent (0.3% and 1%, respectively). Thus the T700SC-12k-60E tow is lightly sized compared to the more heavily sized T700SC-12k-50C. This is noticeable when handling the tows: T700SC-12k-50C is stiff with filaments adhering to each other, while with T700SC-12k-60E, the filaments behave loosely as with unsized tows. These two types were chosen due to their common use in the composites industry and because of the contrast in the amount of sizing between them. An average filament diameter was measured at 6.7 μm in a scanning electron microscope (Zeiss EVO LS15) for both types.

The upper plate and lower platform were made from soda-lime glass for the tow-on-tool tests. The optical semi-reflective coating was deposited on one side of the upper plate (Tofico, France). The optical film has two layers: an 8 nm thick base layer of chromium and an outer 140 nm layer of silica which contacts the filaments. These layer properties were optimised in order to give the best contrast for distinguishing only carbon filaments in contact with the plate; further details are given in Smerdova and Sutcliffe [27]. Surface line-profile data was taken over six scans (scan length and cutoff: 15 mm and 0.08 mm) on each of the upper and lower contact surfaces using a stylus type profilometer (Form Talysurf 120, Taylor Hobson, Leicester, UK). The upper (coated) plate and lower platform had average R_a roughnesses of 0.0044 and 0.0042 μm, respectively. Note that roughness is largely unaffected by the introduction of the coating.

Normal load was recorded by summing the output from the two miniature button load cells (LBS-5, Interface force measurements, Arizona USA) and converted to a nominal pressure p using the appropriate tow nominal contact area. The capacity of the LBS-5 load cells was 22.2 N with nonlinearity, hysteresis and non-repeatability errors being 0.05, 0.05 and 0.1% of the full scale value of 22.2 N, respectively. Tangential force during tow pull-out was measured using a single universal tension/compression load cell (MPL-10, Transducer Techniques, California, USA) mounted between the clamping fixture and the linear stage (Figs. 1 and 2). The MPL-10 load cell had a capacity of 44.4 N with nonlinearity, hysteresis and non-repeatability errors being 0.1, 0.1 and 0.05% of the full scale value of 44.4 N, respectively. The load cells were connected through a full bridge amplifier to a desktop PC via a data acquisition device (National Instruments NI USB-6009) and a LabVIEW program was written to acquire and output the load data.

Images were acquired using a digital camera (Leica DFC295, Leica Microsystems, Switzerland) mounted on an Olympus BX51M microscope. A ×10 objective was used leading to a field of view measuring 1184 μm × 888 μm. At the highest resolution setting this gave images with 2048 × 1536 pixels resulting in a measurement resolution of 0.578 μm. An image stitching procedure within the camera software (Leica Application Suite) was used together with an automated microscope stage to scan an area sufficiently large to be reasonably representative of the entire tow. For the initial tests involving only normal loading, a rectangular scan area consisting of 5 × 8 fields of view (centred in the tow width) was used (i.e. 9.47 mm along the tow by 4.44 mm wide). After further refinement, for the work involving both normal loading and friction force measurement, a scan area large enough to see the entire tow width over a length of seven fields of view was chosen (i.e. 8.3 mm of tow length). Note that the average (unloaded) tow widths for T700SC-12k-60E and T700SC-12k-50C were measured as 7.2 and 5.5 mm, respectively.

2.3. Data processing and analysis

The filament contacts appear as distinctive bright strands in the images as shown in Fig. 3a. There is insufficient resolution to directly measure the true width of the contact patches, but the total length of filament in contact L can be accurately determined. In Smerdova and Sutcliffe [27], a Matlab algorithm to detect the filament contacts and calculate the total contact length was developed and described in detail. Fig. 3b shows the filaments detected by the algorithm for the example image in Fig. 3a. Essentially, a filtering process is carried out whereby a structuring element (or kernel) containing a thin strip is convolved with the images to pick out long thin objects (i.e. the fibre contact regions). This is used to generate a binary image containing contact regions (ones) and non-contact regions (zeros) by employing a suitable threshold. The remaining part of our algorithm differs slightly from Smerdova and Sutcliffe [27]. We use a simple cutoff approach to exclude small lengths (<40.5 μm) of apparent contact which are actually due to interference fringes as a filament departs contact at either end of a contact zone. Finally, we use a morphological thinning method to reduce the contact regions to a skeleton. The total line length of this skeleton corresponds to the total contact length. This contact analysis is carried out separately for each of the images comprising the scanned area, with the overall total contact length being the sum of values from each of the constituent images.

Normal load values were set during the experiments, while the friction force was obtained from the tangential force-displacement curves. In tow-on-tool contact, the maximum value of a well-defined static friction force peak was used, whereas, for the tow-on-tow tests there was often no well-defined static friction peak

Please cite this article in press as: Mulvihill DM et al. Friction of carbon fibre tows. Composites: Part A (2016), http://dx.doi.org/10.1016/j.compositesa.2016.08.034

and the average friction force over a 20 μm sliding distance was used instead. Both static and kinetic friction values are equally applicable for the purposes of this work (i.e. assessing the evolution of friction with normal load – indeed, for the tow-on-tow case the difference between them is not easily distinguishable).

2.4. Test procedure (tow-on-tow)

For the tow-on-tow contact arrangement, a similar experimental procedure was used with the same rig, but with two major differences. First, no optical analysis of the true contact length was possible as the tow-on-tow interface is hidden from view. Second, the set-up around the contact zone was somewhat different. Fig. 4 summarises the set-up used for the three contact types used in the paper. Fig. 4a depicts the tow-on-tool contact arrangement discussed previously, while Fig. 4b and c depict the tow-on-tow setup for parallel and perpendicular tows, respectively. The tow-on-tow arrangement was set up by fixing tows to upper and lower metal plates using double sided adhesive tape. For the parallel arrangement, the fixed tows were positioned parallel to (and in line with) the pull-out tow (Fig. 4b). For the perpendicular configuration, a single layer of fixed tows were laid down side by side at 90° to the pull-out tow (Fig. 4c). For the parallel arrangement, care was taken to make sure that the three tows were accurately lined up and that no adhesive tape was visible at the tow edges. For the perpendicular setup, it was especially important to ensure that no load transfer occurred outside of the intended contact zone. This was achieved by ensuring that the raised lower platform width was only as wide as the pull-out tow. The nominal contact length of tow was 24.25 mm for both parallel and perpendicular tow-on-tow arrangements. With normal load applied, the centre tow was pulled through the two fixed tows in 1 mm increments to measure the friction force at each normal load increment. Again, each test was repeated five times with new tow specimens to give an indication of repeatability.

3. Results and discussion

3.1. Tow-on-tool contact

3.1.1. True contact length – normal loading only

Fig. 5 shows the filaments in contact over the entire scan area for the lowest and highest normal load increments (corresponding to nominal normal pressures p of 0.5 and 245 kPa for the test shown). The result shown is from one of the tests on the T700SC-12k-60E tow. Contact is sparse at 0.5 kPa (Fig. 5a), but has markedly increased by a pressure of 245 kPa (Fig. 5b). Fig. 5b indicates that, at higher pressures, the contact zone tends to consist of dense patches of contact interspersed with areas where the contacts are much less dense. It is interesting also to note that where a filament next to the surface crosses over other filaments, a contact-free area is created around the crossing filament since the surrounding filaments must lose contact in order to pass underneath. A good example of this is circled in Fig. 5b. Most contacting filaments are roughly aligned within ±10° of the nominal tow direction, but a few outlier filaments crossing at markedly steeper angles are present in most of the results (such as that highlighted in Fig. 5b).

The increase in true filament contact length with load is quantified in Fig. 6 for each of the five tests on each tow type. For both types, a distinctive characteristic curve was found where the contact length L increases with normal pressure p as shown. The true contact length is given as a percentage of the idealised contact length assuming a perfect line-up of parallel touching filaments. Values for the true contact length are well below this idealised 100% value. The percentage of idealised contact length (averaged over five tests) varied from 2.4% at 0.6 kPa to 30% at 253 kPa for T700SC-12k-60E tows, and from 0.8% at 0.6 kPa to 25.9% at 305.5 kPa for T700SC-12k-50C tows. The behaviour is repeatable although the magnitudes vary somewhat due to the variability introduced by using a new tow specimen for each test. The stiffer, more highly sized T700SC-12k-50C tow appears to make somewhat less contact than the 'looser' (and lightly sized)

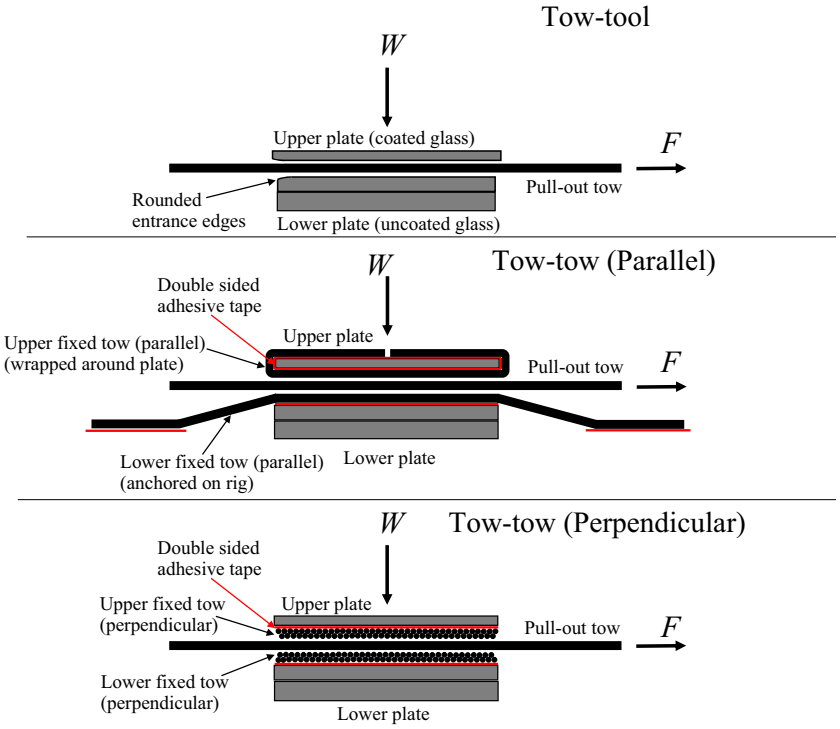

Fig. 4. Three different contact conditions tested: (a) tow-on-tool, (b) tow-on-tow (parallel) and (c) tow-on-tow (perpendicular). (For interpretation of the references to colour in this figure legend, the reader is referred to the web version of this article.)

Please cite this article in press as: Mulvihill DM et al. Friction of carbon fibre tows. Composites: Part A (2016), http://dx.doi.org/10.1016/j.compositesa.2016.08.034

T700SC-12k-60E tow - see Fig. 6. Clearly, this evolving contact length with pressure must be incorporated in future tow contact models rather than assuming an idealised contact arrangement.

3.1.2. True contact length and friction – normal loading with tangential pull-out

Contact length. Fig. 7 shows the variation of true contact length with pressure for the tests which involved both normal and tangential loading. In these tests, the tow is pulled out by a distance of 1 mm at each normal load increment and a tangential force equal to the limiting friction force develops. Here, the percentage of idealised contact varied from an average of 1.4% at 0.5 kPa to 32% at 264.5 kPa for T700SC-12k-60E and from 0.4% at 0.6 kPa to 36.2% at 326.6 kPa for T700SC-12k-50C. The overall behaviour is similar to the graph in Fig. 6 for normal loading only, but with a few notable differences: there seems to be less difference in contact length magnitude between the two tow types at the higher pressures, somewhat less variability in the results, and finally, a more marked transition is evident at around 50 kPa where the rate of change of contact length changes. The change in slope at 50 kPa is indicative of a change of filament packing regime of the kind noted for the compression of fibrous preforms in Chen et al. [30]. The tendency of the tangential loading to line up the filaments and alter the filament arrangement may be responsible for the subtle differences between Figs. 6 and 7. These differences are relatively unimportant, however, as it is the characteristic increase in filament contact length with pressure behaviour that will prove to be a key element in understanding the frictional behaviour of the tows.

Contact area, interface strength and friction. Before exploring the physical mechanisms underlying the frictional behaviour, we turn to the experimental friction results. Fig. 8 plots friction force versus normal load and Fig. 9 shows the friction coefficient plotted against normal pressure. It is immediately clear that the T700SC-12k-50C tow gives a friction force about 1.5 times the value for the T700SC-12k-60E tow – we will return to this point later. It is also evident that the tow friction force (Fig. 8) does not obey Amonton's law, but follows the more general power law description $F = kW^n$ with the friction coefficient f (Fig. 9) following the corresponding inverse power law relation ($f = kW^{n-1}$). The first row of Table 1 gives the mean values of the fitting coefficients k and n based on the five tests on each tow type (coefficients were calculated using a least squares fitting approach in Matlab). These values give (on average) a friction force proportional to $W^{0.72}$ for T700SC-12k-60E and to $W^{0.83}$ for T700SC-12k-50C. These particular variations with normal load require some explanation; hence, we turn to the underlying contact mechanics of the carbon filaments and the well-established adhesion theory of friction.

The adhesion theory models friction as arising from an adhesion shear stress τ acting across the real contact area A:

$$F = \tau A \tag{1}$$

This shear stress is generally thought of as being equal to the shear strength of the individual bonded junctions (i.e. a constant). Therefore, if Eq. (1) holds for the tows, it is the variation of real contact area A with normal load W which will determine the form of the F–W relation. As mentioned above, our technique does not allow direct measurement of the actual contact area under the filaments. However, this can be estimated from knowledge of the filament properties and the 'evolving contact length' measurements discussed above. Fig. 10 shows scanning electron microscope (SEM) images of filaments from each tow type. The T700SC-12k-60E filaments (Fig. 10a and b) can clearly be approximated as

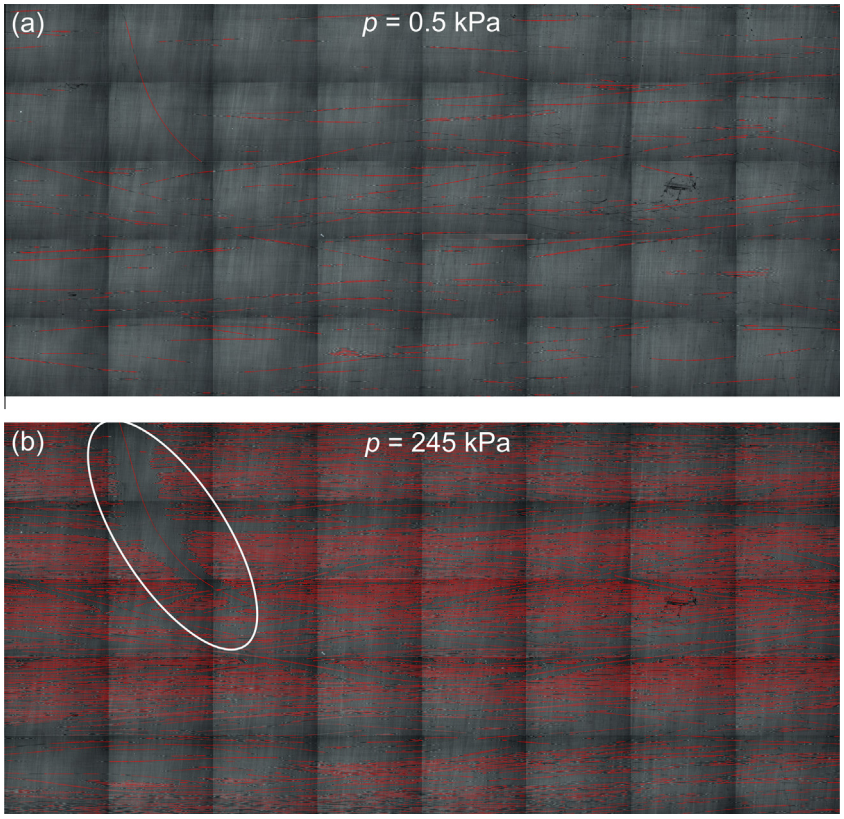

Fig. 5. Post-processed montage images of overall scan-area showing detected filament contacts (in red) for (a) normal pressure $p = 0.5$ kPa (first load increment) and (b) normal pressure $p = 245$ kPa (final load increment). Results are from one of the five tests on T700SC-12k-60E with normal loading only. The contact effect due to a filament crossing over other filaments is highlighted in (b). (Scan area size: 4.44 mm × 9.47 mm). (For interpretation of the references to colour in this figure legend, the reader is referred to the web version of this article.)

Please cite this article in press as: Mulvihill DM et al. Friction of carbon fibre tows. Composites: Part A (2016), http://dx.doi.org/10.1016/j.compositesa.2016.08.034

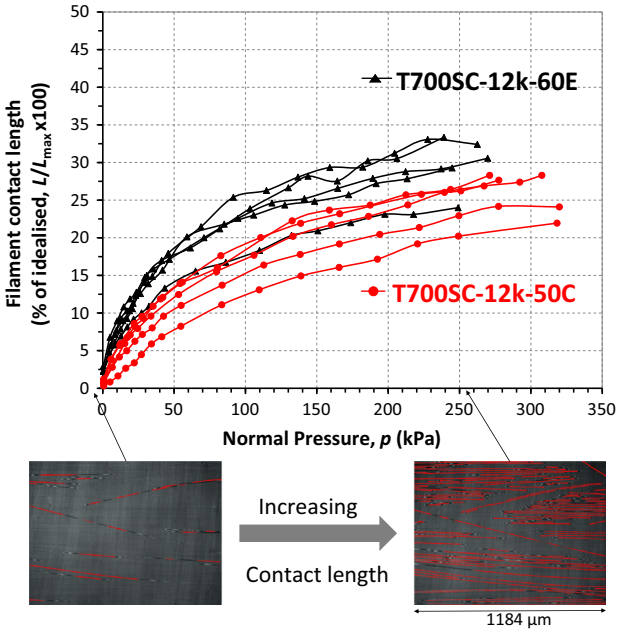

Fig. 6. True filament contact length L as a percentage of the idealised maximum L_{max} (i.e. assuming parallel touching filaments) versus nominal pressure p in tow-on-tool contact for tows: T700SC-12k-60E and T700SC-12k-50C under normal loading only. Five test results shown for each tow type (new tow specimen for each test). Example image (single field of view) from beginning and end of one of the tests on T700SC-12k-60E shown. (For interpretation of the references to colour in this figure legend, the reader is referred to the web version of this article.)

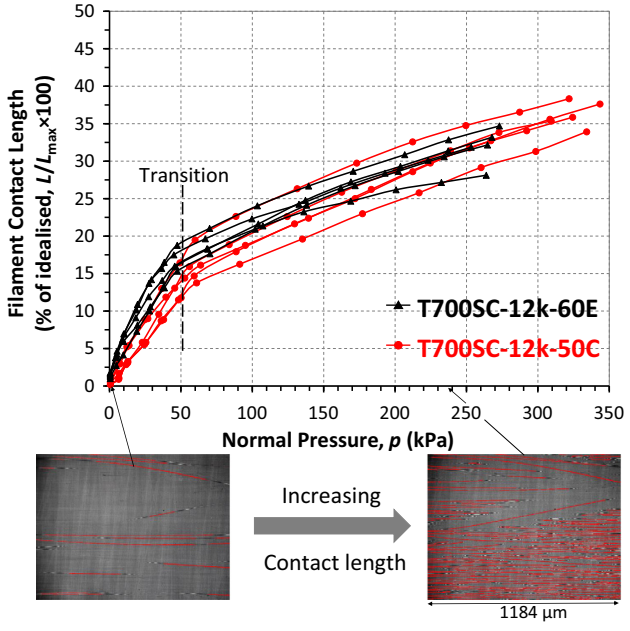

Fig. 7. True filament contact length L as a percentage of the idealised maximum L_{max} (i.e. assuming parallel touching filaments) versus nominal pressure p in tow-on-tool contact for tows: T700SC-12k-60E and T700SC-12k-50C under normal *and* tangential loading. Five results shown for each tow type (new tow specimen for each test). Example image (single field of view) from beginning and end of one of the tests on T700SC-12k-60E shown. (For interpretation of the references to colour in this figure legend, the reader is referred to the web version of this article.)

smooth elastic cylinders of carbon, while treatment of the T700SC-12k-50C filaments is made more difficult by the presence of a substantial coating (i.e. the sizing visible in Fig. 10c and d). The higher sizing amount on the T700SC-12k-50C tows was also evident in the gaps between filaments where the sizing can be seen sticking

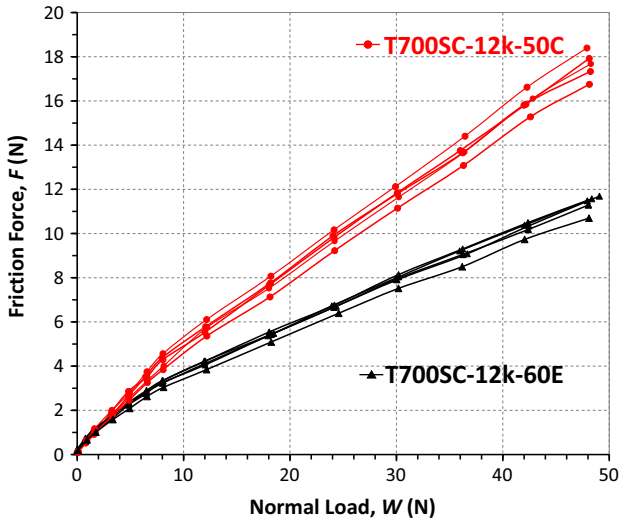

Fig. 8. Friction force F versus normal load W for tow-on-tool contact with T700SC-12k-60E and T700SC-12k-50C. Five results shown for each tow type (new tow specimen for each test). (For interpretation of the references to colour in this figure legend, the reader is referred to the web version of this article.)

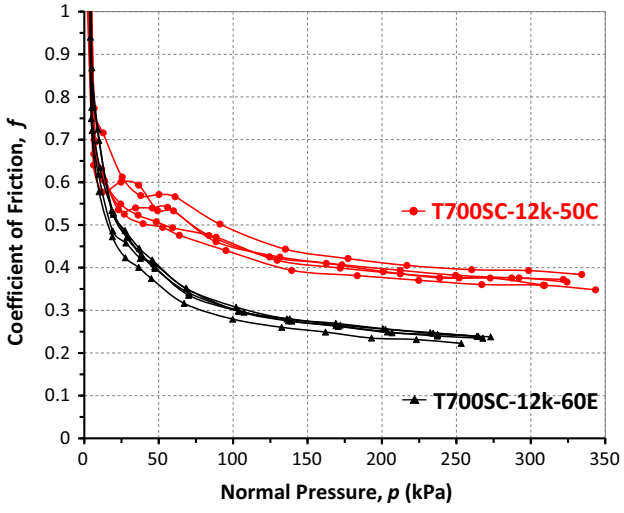

Fig. 9. Coefficient of friction f versus normal pressure p (nominal) for tow-on-tool contact with T700SC-12k-60E and T700SC-12k-50C tows. Five results shown for each tow type (new tow specimen for each test). (For interpretation of the references to colour in this figure legend, the reader is referred to the web version of this article.)

individual filaments together as can be seen in Fig. 10c and d. Hence, we proceed with an analysis based on the T700SC-12k-60E tow. Since the filaments make contact with smooth glass plates in the experiment, we can idealise the contact as a classic cylinder-on-flat Hertzian case where the contact half-width a is given by:

$$a = \left(\frac{2Wd}{\pi E^* L}\right)^{1/2} \tag{2}$$

where W is the total normal load on the contact patch, d is the filament diameter, E^* is the effective elastic modulus and L is the total length of filament in contact. The effective modulus is calculated from the elastic moduli E_{CF} and E_{Glass} and Poisson's ratios ν_{CF} and ν_{Glass} of the carbon fibre and glass, respectively:

$$\frac{1}{E^*} = \frac{1-\upsilon_{Glass}^2}{E_{Glass}} + \frac{1-\upsilon_{CF}^2}{E_{CF}}. \tag{3}$$

Table 1
Mean power law fitting coefficients for the friction force–load plot (i.e. $F = kW^n$) based on all five tests in tow-on-tool and tow-on-tow (parallel and perpendicular) configurations. For T700SC-12k-60E, coefficients are also given for the area–load curve (i.e. $A = kW^n$). Bracketed values are standard deviations.

	T700SC-12k-60E		T700SC-12k-50C	
Plot type	k	n	k	n
Tow-on-tool ($F = kW^n$)	0.70 (0.037)	0.72 (0.008)	0.71 (0.055)	0.83 (0.015)
Tow-on-tool ($A = kW^n$)	0.04 (0.004)	0.72 (0.026)	–	–
Tow-on-tow, parallel ($F = kW^n$)	0.36 (0.013)	0.87 (0.012)	0.73 (0.10)	0.90 (0.042)
Tow-on-tow, perpendicular ($F = kW^n$)	0.17 (0.014)	0.94 (0.034)	0.18 (0.005)	0.96 (0.019)

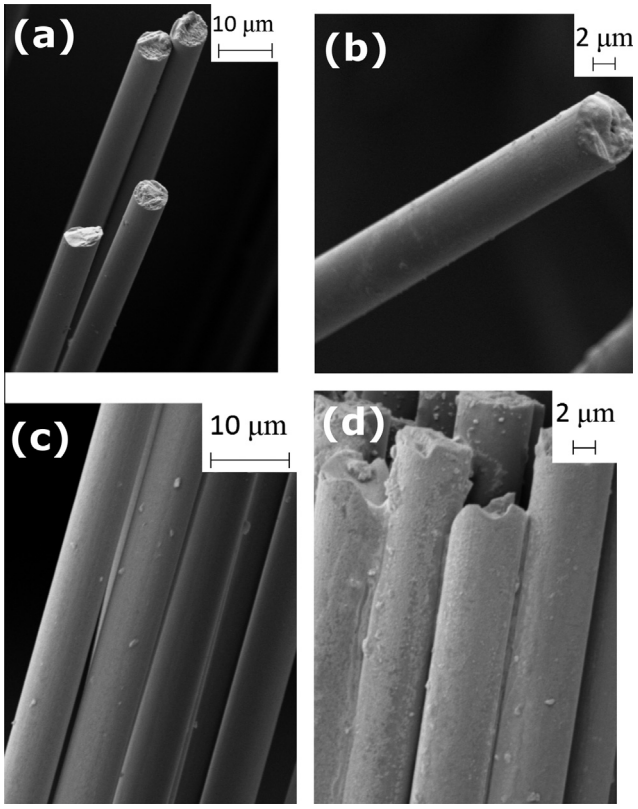

Fig. 10. Scanning electron microscope (SEM) images of: (a and b) T700SC-12k-60E and (c and d) T700SC-12k-50C filaments.

Owing to the way the filaments were loaded, E_{CF} = 16.5 GPa and ν_{CF} = 0.31 were taken as the transverse elastic modulus and Poisson's ratio of the carbon filaments as determined using laser resonant ultrasound spectroscopy by Mounier et al. [31] for T700 filaments. Standard properties of E_{Glass} = 69 GPa and ν_{Glass} = 0.24 were used for the glass [32]. The real contact area is then given by:

$$A = 2aL. \tag{4}$$

Fig. 11 plots contact area from Eq. (4) against normal load for each of the five repeat tests on T700SC-12k-60E. If we assume the idealised arrangement of parallel touching filaments, then the contact length L remains constant and we obtain a contact area proportional to $W^{1/2}$ (dashed lines in Fig. 11). It follows then from Eq. (1) that the friction force would also be proportional to $W^{1/2}$, but this is not borne out in the experimental results where the average value of the exponent is 0.72 for T700SC-12k-60E (first row of Table 1). However, if we include the evolving 'real' contact length from Fig. 7 in the calculations in Eqs. (2) and (4), the exponent n increases and the resulting curve 'straightens' as shown by the lower plot in each part of Fig. 11. Values of the coefficients for curve-fits $A = kW^n$ to these plots are given in the second row of Table 1 (the curve fit is shown by the undashed line on Fig. 11). The mean value of the exponent n is now 0.72 which agrees closely with the mean exponent from the measured F–W curves (also approximately 0.72). Since the exponents are similar, the A–W and F–W curves clearly differ only by a constant factor. Thus the tow behaviour agrees with the 'adhesion' or 'constant interface strength' model of friction (i.e. $F = \tau A$) and we can multiply the contact area curves in Fig. 11 by a constant 'interface strength' τ to recover the friction force. Fig. 12 plots both the measured friction force curves (i.e. F–W) and the curves obtained from multiplying the real contact area curves in Fig. 11 by a suitable constant (i.e. τA–W). The values of τ required to reproduce a reasonable fit to the friction data in each of the five tests were: 16.5, 16, 17, 15.5 and 15 MPa. This gives an average interface strength of 16 MPa over the five tests. Note that a value of interface strength as high as 16 MPa comes about because the actual real area of contact is so small: the average contact area over the five tests was only 0.7 mm^2 at the highest test pressure (Fig. 11). Since the nominal area of the contact patch at this pressure was 183 mm^2, this represents only 0.4% of the total. Our value for τ is close to the value of 15 MPa calculated in a similar way by Roselman and Tabor [15] for *single* carbon filaments of fixed contact length in contact with smooth stainless steel surfaces (R_a up to 0.26 μm). Although this is encouraging, it should be acknowledged that these values are guideline approximations only as we have assumed Hertzian contact in calculating the real contact area and because the inevitable presence of small scale nano-roughness on the filaments and even on the apparently smooth glass will tend to reduce the real contact area. Thus, 15 MPa is likely to be a lower bound and the 'real' interface strength may be somewhat higher. Although a calculation of the correct contact area magnitudes for the T700SC-12 k-50C tows is complicated by the presence of significant sizing, we find the same similarity between the F–W and F–A curves when we treat the filaments as idealised carbon cylinders as above.

Our experimental approach here has been at the *multi-filament* tow level and we have used accurate measurements of real filament contact length to estimate the real contact area under the filaments (using theory) and infer a shear strength τ (using the total measured friction force). However, a smaller scale experimental approach would be required to *directly* measure the real contact area and estimate τ more accurately. Such a study might involve sliding a short length of *single filament* in a suitable Atomic Force Microscope, measuring the real contact area by some novel technique (such as via the indentation produced or the conductivity of the interface), and detecting the small limiting friction forces that arises when the portion of filament enters the sliding regime.

The most important point to note, however, is not the exact magnitudes for τ, but that the above contact area analysis predicts the correct form of the F-W curve. Assuming an idealised arrangement of filaments (constant contact length) within a Hertzian analysis predicts an incorrect variation with W, but taking account of the evolving 'real' contact length produces exactly the right shape (i.e. the correct exponent in $F = kW^n$). The explanation is analogous to Greenwood and Williamson's approach [19] to explaining why rough surfaces of elastically deforming (spherical) asperities do not follow the elastic predictions for a friction force proportional

Please cite this article in press as: Mulvihill DM et al. Friction of carbon fibre tows. Composites: Part A (2016), http://dx.doi.org/10.1016/j.compositesa.2016.08.034

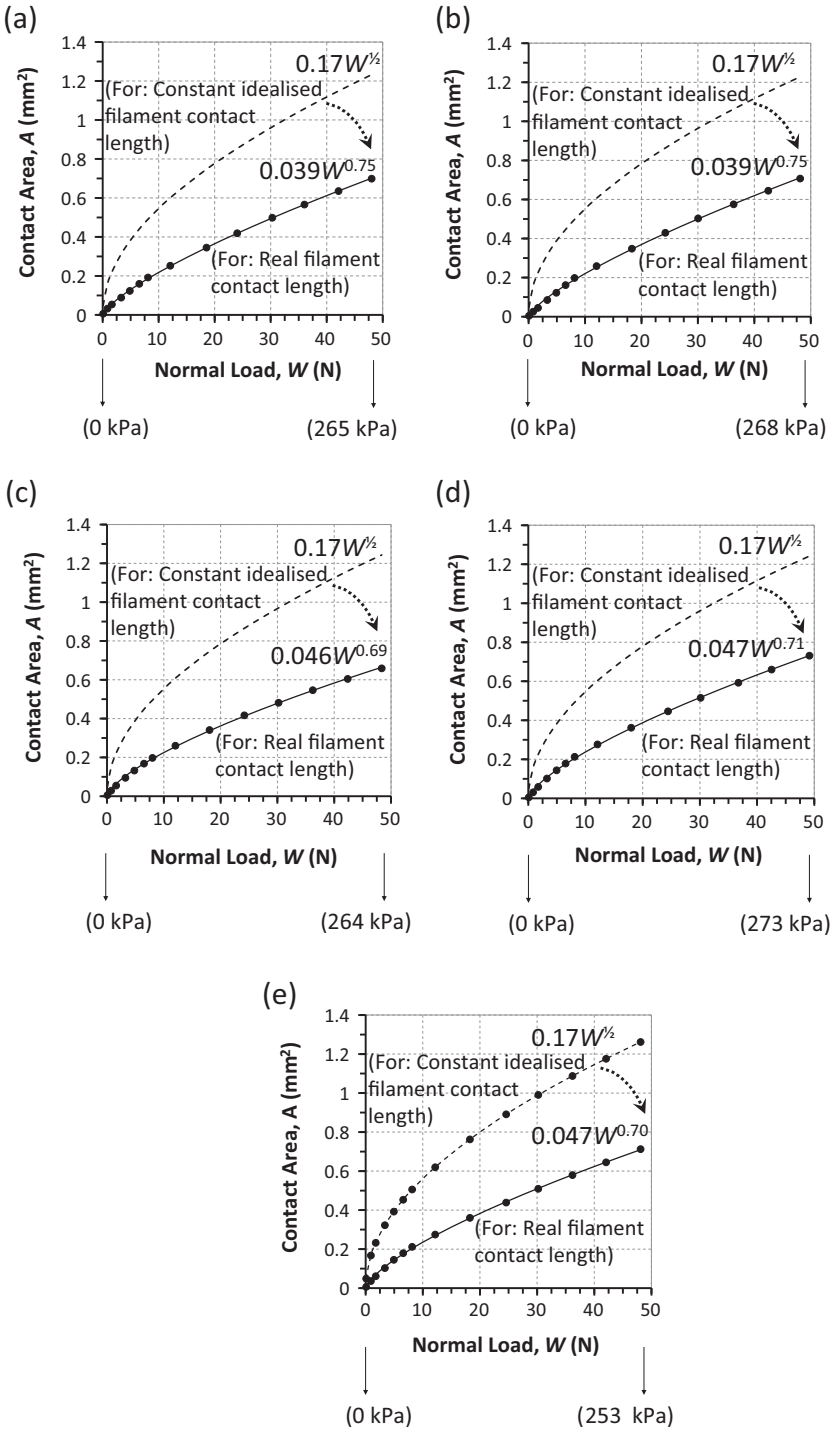

Fig. 11. Total contact area *A* versus normal load *W* for T700SC-12k-60E. Calculated from cylinder-on-flat Hertz formula for both constant idealised filament contact length and for the evolving 'real' filament contact length from Fig. 7. Figures (a–e) show the five repeat tests (a new tow specimen was used for each test). Total nominal contact area at final load increment: 183 mm^2.

to $W^{2/3}$, but rather give almost directly proportionality with *W* (i.e. Amonton's law). They realised that if the effect of increasing the load was to make existing elastic contacts grow, there will not be direct proportionality, but if the effect is primarily to form new contacts, there may well be. In the case of a fibrous tow contacting a flat surface, the addition of new contact length with pressure is equivalent to the formation of the new asperity contacts in Greenwood and Williamson. This pushes the exponent *n* away from the local Hertzian prediction of either 1/2 or 2/3 and closer to unity for the overall contact patch. Based on the experiments here, and on measurements elsewhere in the literature [24], it appears that unlike conventional metal surfaces (obeying Amonton's Law), the exponent in the case of fibrous tows seems to lie somewhat less than unity in the range 0.7–1. This is probably because the underlying cylindrical geometry of the filaments enforces some degree of non-linearity despite the counter-effect of the increasing contact length. Returning back to Fig. 11 we can see that, if idealised tow contact is assumed, the magnitudes of the predicted friction forces would also be incorrect since the idealised arrangement significantly over-predicts the real contact area.

Please cite this article in press as: Mulvihill DM et al. Friction of carbon fibre tows. Composites: Part A (2016), http://dx.doi.org/10.1016/j.compositesa.2016.08.034

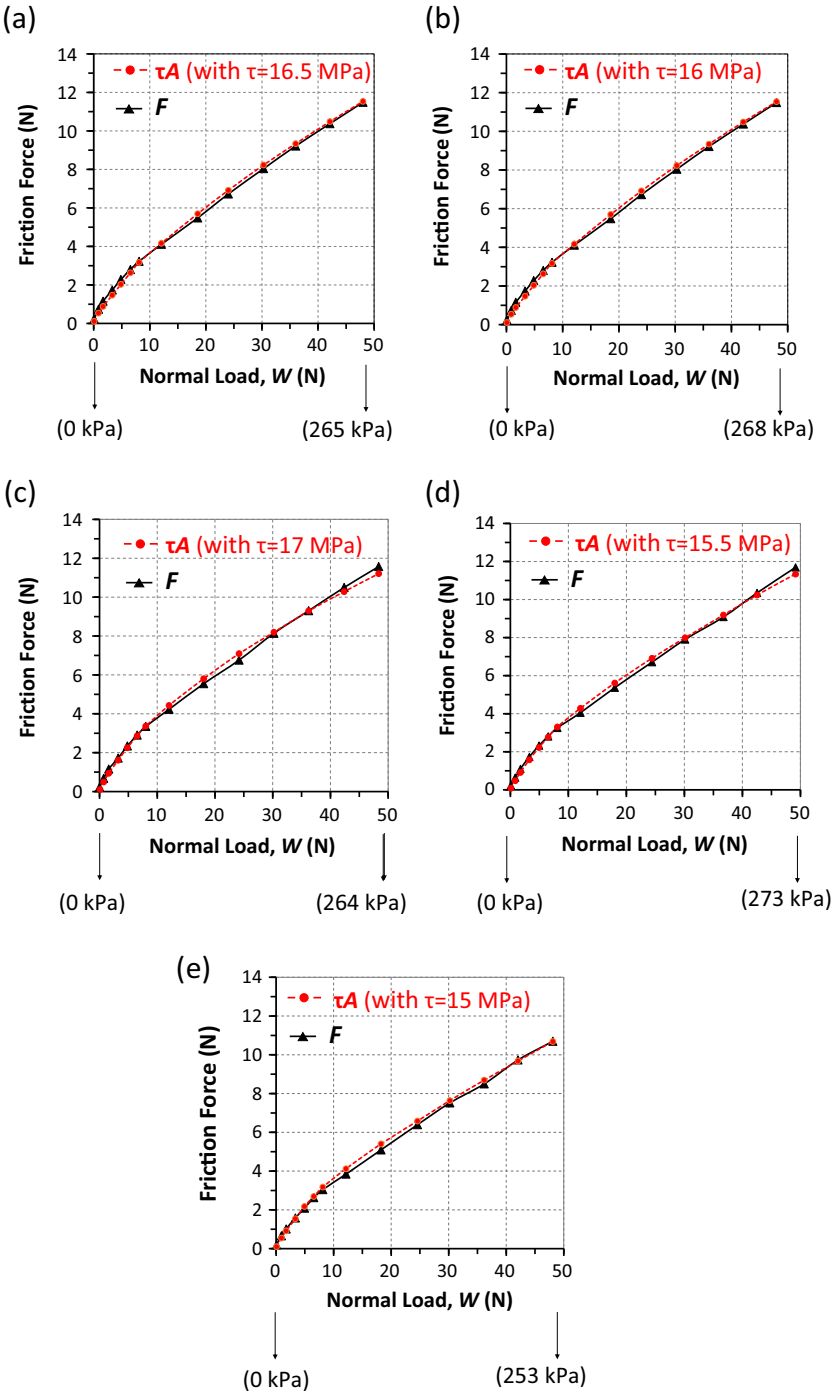

Fig. 12. Measured friction force F versus normal load W. Contact area A (from Fig. 11, based on real contact length) times a suitable shear strength τ yields a curve which closely overlays the measured friction force F. (a–e) show the five repeat tests on T700SC-12k-60E (a new tow specimen was used for each test). (For interpretation of the references to colour in this figure legend, the reader is referred to the web version of this article.)

Finally, we return to the observation that the friction was about 1.5 times higher for T700SC-12k-50C than for T700SC-12k-60E (Figs. 8 and 9). Our analysis in terms of real contact area is likely to apply again here: the T700SC-12k-50C filaments are heavily coated (see SEM images in Fig. 10), and, therefore, it is most likely that they produce a greater 'real' contact area and, hence, greater friction. Assuming the sizing deforms plastically compared to the substrate carbon, we can make a very rudimentary estimate of the contact area of sizing (for a given tow type) by assuming that the half-width a of sizing in contact is constant once a small critical load is reached and is given by the length of horizontal plane crossing through half of the annular sizing region once the plane is touching the carbon filament (inner circle) as illustrated in Fig. 13. From Section 2.2, the difference in volume of sizing present between T700SC-12k-50C and T700SC-12k-60E is 3.3 (or 1/0.3) if we assume similar densities for the two sizing types. By the geometry of Fig. 13, the square of the half-width a is proportional to the annular volume of sizing per unit length given by $\pi(r_o^2 - r_i^2)$. Thus, if the volume of sizing changes by a factor of 3.3, the half width a (and hence the real contact area of sizing) should change by $\sqrt{3.3} = 1.8$ which corresponds reasonably well with the frictional

Please cite this article in press as: Mulvihill DM et al. Friction of carbon fibre tows. Composites: Part A (2016), http://dx.doi.org/10.1016/j.compositesa.2016.08.034

change of about 1.5 between the two tow types. This estimate of how a change in sizing amount might affect sizing contact area offers a guideline only due to the assumptions made. We should point out here also that the sizing types are somewhat different between T700SC-12k-60E and T700SC-12k-50C (see Section 2.2) and therefore a contribution to the friction difference caused by the chemistry related adhesion properties of the sizing is a possibility. In any case, we see that sizing can have a significant effect on friction. We should note that the friction coefficients in Fig. 9 are from tows contacting very smooth glass surfaces (R_a = 0.004 - μm). Based on a recent study (Mulvihill and Sutcliffe [22]) of the effect of tool surface roughness on tow friction, we might expect the values here to be about twice those that could be expected with common rough metal surfaces having roughness values greater than about 0.1 μm – this is because very smooth surfaces (R_a < 0.1 μm) allow a greater true filament-tool contact area.

3.2. Tow-on-tow contact

In tow-on-tow contact, the friction force required to pull-out a middle tow from between two fixed tows at various normal loads was measured and the procedure was described in Section 2.4. Figs. 14 and 15 plot friction force against normal load for each tow type in the tow-on-tow parallel and perpendicular arrangements, respectively. The fitting coefficients corresponding to a fit of $F = kW^n$ to the data are shown in the last two rows of Table 1. Again, treating the filaments as idealised arrangements of touching cylinders, a Hertzian analysis would predict a $W^{1/2}$ dependency for the friction force in the parallel case and a $W^{2/3}$ dependency for the perpendicular case. As was the case for the tow-on-tool tests, this was not borne out experimentally and the mean exponents n in the parallel and perpendicular arrangements, respectively, were 0.87 and 0.94 for T700SC-12-60E and 0.90 and 0.96 for T700SC-12k-50C (third and fourth rows of Table 1). Although the contact interface between the tows could not be observed during the test as for the tow-on-tool experiments above, it is likely that the same underlying behaviour causes the exponent to be greater than the idealised prediction. Namely that, for the parallel arrangement, 'real' filament contact length probably increases with normal load much like in Fig. 7, and that, for the perpendicular case, the number of crossed-cylinder 'point contacts' increases with load in an analogous manner – the addition of 'new contact' in conjunction with the elastic widening of existing contacts being the reason for the exponent being pushed closer to unity. It is not surprising that the exponents in the perpendicular case are closer to unity (fourth row of Table 1), than for the parallel case as, even in the idealised setup (with no new contact length or contact points coming into play), the exponent would be greater for the perpendicular case – i.e. 2/3 (perpendicular) as opposed to 1/2 (parallel). Actually, with mean exponents of 0.94 and 0.96, the tows in the perpendicular arrangement are close to obeying Amonton's Law. It would be interesting to try to observe the suggested increase in contact length (parallel arrangement) and number of contact patches (perpendicular arrangement) with normal loading in tow-on-tow contact, but this presents a significant experimental challenge.

The T700SC-12k-50C tow also produces higher friction forces than the T700SC-12k-60E tow in tow-on-tow contact (about 2.2 times as much in the parallel arrangement – Fig. 14) and this is again likely due to the existence of a greater contact area produced by the heavy sizing on T700SC-12k-50C (again, a contribution due to differences in sizing chemistry cannot be ruled out). The difference was much less in the perpendicular arrangement (only about 1.2 times – Fig. 15); this is difficult to explain though it may be due to the sizing playing less of a role at the localised 'point contacts' in the perpendicular arrangement as opposed to the continuous 'line contacts' in the parallel arrangement. This may be because the

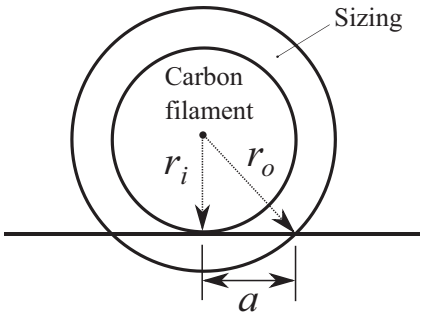

Fig. 13. Rudimentary approach to making an estimate for how sizing contact width (twice the half-width a) changes with annular volume of sizing.

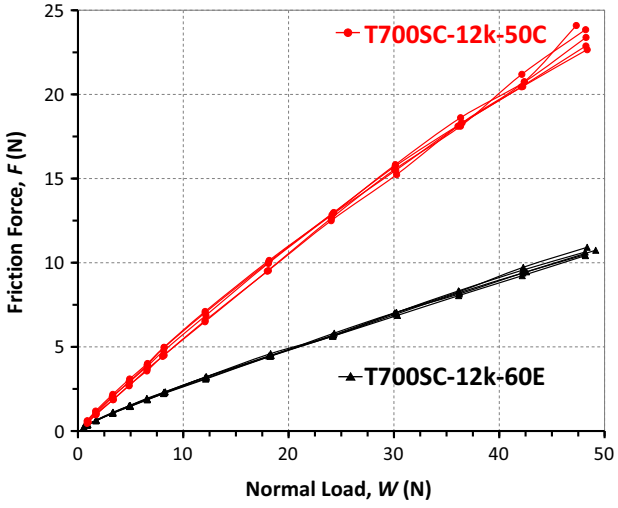

Fig. 14. Friction force F versus normal load W for tow-on-tow contact in the parallel arrangement. Five results shown for each tow type (i.e. T700SC-12k-60E and T700SC-12k-50C). (For interpretation of the references to colour in this figure legend, the reader is referred to the web version of this article.)

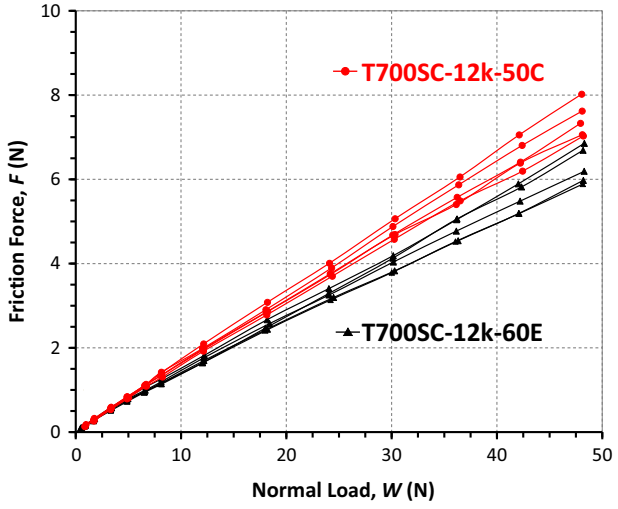

Fig. 15. Friction force F versus normal load W for tow-on-tow contact in the perpendicular arrangement. Five results shown for each tow type (i.e. T700SC-12k-60E and T700SC-12k-50C). (For interpretation of the references to colour in this figure legend, the reader is referred to the web version of this article.)

Please cite this article in press as: Mulvihill DM et al. Friction of carbon fibre tows. Composites: Part A (2016), http://dx.doi.org/10.1016/j.compositesa.2016.08.034

point contacts allow the sizing to be pushed aside into the gaps between them, while in the line contact case, the sizing is trapped within the inter-tow contact zone along the entire contact patch – this requires further investigation.

Fig. 16 plots the variation of friction coefficient with normal pressure for the tow-on-tow tests on T700SC-12-60E (Fig. 16a) and T700SC-12k-50C (Fig. 16b). In both cases, the parallel tow arrangement gives a significantly higher friction coefficient. For T700SC-12k-60E, the difference was about 1.7 times at the maximum test pressure (about 272 kPa), while for T700SC-12k-50C, friction was as much as 3.2 times greater in the parallel arrangement at the same test pressure. This sensitivity of friction to tow orientation (with friction increasing as the tows go from perpendicular to parallel) has also been found by Cornelissen et al. [24] and Chakladar et al. [26]. Again, we turn to a consideration of the 'real' contact area to offer an explanation. Considering the filaments as an array of elastic cylinders packed in an idealised manner (i.e. parallel touching filaments), we can calculate the real contact area A for a region of tow-on-tow contact in both the parallel and perpendicular contact configurations using a simple Hertzian analysis. The schematic inset in Fig. 17 depicts the theoretical setup. We consider a square nominal contact patch of side equal to Nd, where d is the filament diameter and N is the number of contacting filaments in each surface layer. The total 'real' contact area within the square patch for the parallel arrangement, $A_{||}$, is then easily derived from the Hertz formula for contacting parallel cylinders as:

$$A_{||} = 4N^2 d^2 \left(\frac{p}{2\pi E'}\right)^{1/2}, \tag{5}$$

where E' is the plane strain modulus $E/(1-\nu^2)$ and p is the nominal contact pressure (i.e. total inter-tow normal force divided by the nominal contact area N^2d^2). Contact area in the perpendicular arrangement, $A_{\perp}$, is calculated from the Hertz formula for crossed cylinders as:

$$A_{\perp} = \pi N^2 d^2 \left(\frac{3p}{4E'}\right)^{2/3}. \tag{6}$$

Dividing Eq. (5) by Eq. (6) yields an expression for the contact area ratio:

$$\frac{A_{||}}{A_{\perp}} = \frac{4}{\pi}\sqrt{\frac{2}{3\pi}}\left(\frac{4E'}{3p}\right)^{1/6}. \tag{7}$$

The contact area ratio is plotted against nominal pressure p in Fig. 17. (The plane strain modulus was calculated from the transverse modulus value of $E = 16.5$ GPa for T700 filaments with $\nu = 0.31$ [31].) Since friction force is proportional to real contact area in the adhesion theory understanding of friction (Eq. (1)), Fig. 17 explains why higher friction coefficients are always measured for tow-on-tow contact in the parallel arrangement. Essentially, the parallel arrangement produces a greater real contact area (at equivalent pressures) and, therefore, a higher friction coefficient. It is instructive to compare an experimental result to the corresponding theoretical magnitudes predicted in Fig. 17. For the test pressure discussed above (272 kPa), Fig. 17 predicts a contact ratio of 3.9. Thus the T700SC-12k-50C tows (contact ratio 3.2) are close to the theoretical prediction while the T700-12k-60E tows (contact ratio 1.7) deviate from the theory in terms of the relative magnitudes. However, we know from our work on tow-on-tool contact that the actual filament arrangement deviates significantly from the idealised configuration and, therefore, we can also expect some differences in the measured results. Overall, though, the analysis in terms of relative contact area appears to offer a robust explanation for the sensitivity to inter-tow orientation.

4. Conclusions

The dry forming process for composite materials involves the pressing of layers of carbon fabric material into a desired shape by a tool prior to resin infusion. This paper focuses on the fundamental frictional behaviour of the fibrous tows comprising the fabrics. Two tow types were studied (a lightly sized tow and a heavily sized one) in both tow-on-tool and tow-on-tow contact.

For tow-on-tool contact, an experiment allowing simultaneous measurement of the 'true' filament contact length and the friction force over a range of normal loads was devised. Contact length observations were facilitated by making observations through a glass plate with a specialised semi-reflective coating. Far from having the previously assumed constant idealised contact length (based on touching parallel filaments), distinctive characteristic curves showing how the 'true' contact length evolves with normal pressure were found. For example, in a set of tests on the lightly sized tow, the average contact length, expressed as a percentage of the idealised contact length, varied from 1.4% at 0.5 kPa to 32% at 265 kPa. The friction force F versus normal load W curves followed power law descriptions ($F = kW^n$) with, on average, F being proportional to $W^{0.72}$ for the lightly sized tow and to $W^{0.83}$ for the heavily sized tows. These variations with normal load were explained by considering how the 'real' contact area varies with load. Real contact area could not be measured directly, but was calculated using a Hertzian cylinder-on-flat analysis for the lightly sized tow in contact with the smooth glass surface. Assuming the idealised *constant* filament contact length, this predicts an area

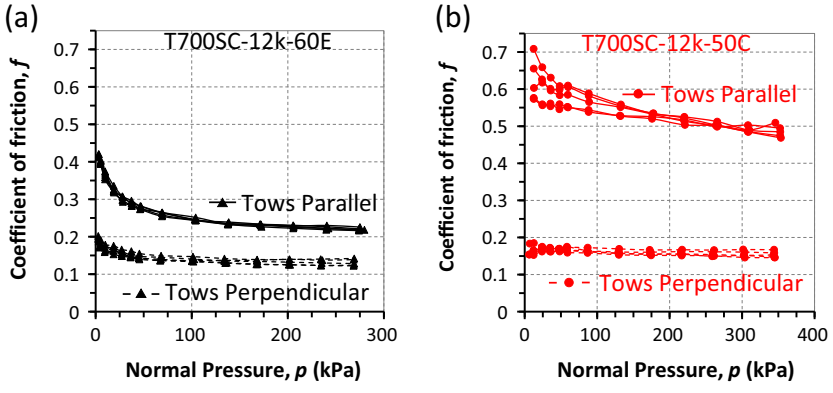

Fig. 16. Coefficient of friction f versus normal pressure p (nominal) for tow-on-tow contact in the parallel and perpendicular arrangement for: (a) T700SC-12k-60E and (b) T700SC-12k-50C tows. Five repeat results shown for each tow type in each arrangement. (For interpretation of the references to colour in this figure legend, the reader is referred to the web version of this article.)

Please cite this article in press as: Mulvihill DM et al. Friction of carbon fibre tows. Composites: Part A (2016), http://dx.doi.org/10.1016/j.compositesa.2016.08.034

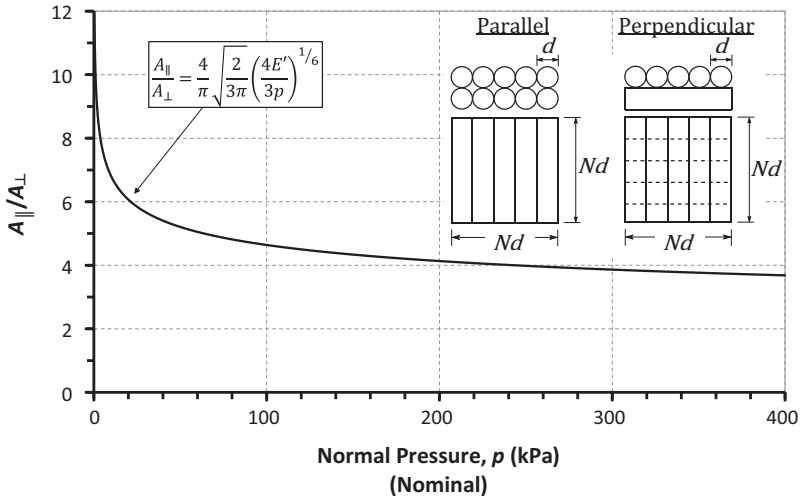

Fig. 17. Theoretical relationship between contact areas for idealised parallel and perpendicular tow-on-tow arrangements (i.e. $A_\parallel/A_\perp$) based on simple Hertzian analysis. The contact patch is a square of size Nd where N is the number of filaments in each surface layer, d is the filament diameter, p is the nominal normal pressure over the entire contact patch and E' is the plane strain modulus for the T700 filaments used in the present study.

proportional to $W^{1/2}$ which differs from the experimental friction force variation. However, when the measured 'true' contact length was included in the calculation, almost exactly the right variation with normal load was found. Essentially, the addition of 'new contact length' forces the power law exponent to be greater than the constant contact length Hertzian prediction of 1/2. This is analogous to the Greenwood and Williamson observation that, for rough surfaces with elastically deforming asperities, the exponent in the global area-load dependency will be greater than the exponent occurring at the local (Hertzian) asperity contacts *only* if the application of load produces new contacts. The increasing filament 'contact length' with load behaviour which we have found is essentially the missing link between theory and experiment in the same way that the increasing number of contacts with load was for Greenwood and Williamson's metal surfaces. Since the area curves and the friction force curves differed only by a constant factor, the results are in agreement with the 'adhesion' or 'constant interface strength' model of friction. For the lightly sized tow, the average 'interface strength' was calculated at 16 MPa.

In tow-on-tow contact, each tow type was tested in two arrangements: filaments parallel and filaments perpendicular. The friction force again followed a power law variation with normal load and the average exponent was in the range 0.87–0.96 for the four test types. Here, although the contact itself could not be observed, we assume the same mechanism for the deviation from the Hertzian prediction as occurred for tow-on-tool contact. Namely, that the true contact length increases with load for the parallel arrangement and that the number of contact points increases with load for the perpendicular arrangement; thereby, pushing the exponent towards unity. In agreement with previous studies, it was also found that friction coefficient is sensitive to tow orientation – being higher for the parallel arrangement (by 1.7–3.2 times). This was explained by considering the real contact area and performing simple Hertzian calculations on an array of filaments forming an idealised patch of tow-on-tow contact. Essentially, the parallel arrangement predicts a greater contact area for the same nominal pressure on the contact patch – hence, higher friction.

Finally, the amount of sizing was found to also affect the friction magnitudes in both tow-on-tool and tow-on-tow contact. The heavily sized tow gave friction coefficients as much as twice those for the lightly sized tow. Here, again, the most likely explanation is in terms of contact area i.e. that the heavily sized tow gives rise to a greater contact area and thus higher friction (although some contribution due to differences in sizing chemistry may also be present).

Clearly, predictive models of tow and fabric contact and friction must account for these findings: especially the evolving contact length and the agreement with the 'constant interface strength' model of friction (i.e. dependence of friction on the real contact area). Further advancement in this area is likely to come about by also studying both the lower and higher levels of hierarchy. A detailed small-scale experimental study (perhaps in a suitable Atomic Force Microscope) of the 'real' contact area and friction forces produced by short lengths of individual filaments in filament-filament and filament-tool contact would be useful in further refining predictions of the interface strength τ, while ways to incorporate the tow behaviour discussed here in macro-scale fabric interactions is also required.

Acknowledgements and additional information

The authors would like to acknowledge the assistance of the Engineering and Physical Sciences Research Council (EPSRC) for supporting the present work under grant Ref. EP/K032798/1 (Friction in Composites Forming). We would also like to acknowledge the contribution of our industrial collaborators at Jaguar Land Rover and Granta Design Ltd, as well as our academic partners from the Composites Research Group at the University of Nottingham (Dr Endruweit and Profs. Long, Warrior and De Focatiis). Hexcel UK are thanked for supplying the tow material. The detailed data relating to this paper can be accessed at the following Cambridge Data Repository: http://dx.doi.org/10.17863/CAM.1671.

References

[1] Kaiser D. Markets: aerospace to consume $57 billion of composites between 2007 and 2026. Adv Compos Bull (AUG.) 2007:12.
[2] Bhattacharyya SK. Smarter–lighter–greener: research innovations for the automotive sector. Proc R Soc London A: Math, Phys Eng Sci, 471(2179).
[3] Howell HG, Mazur J. Amonton's law and fibre friction. J Textile Inst Trans 1953;44(2):T59–69.
[4] Huffington JD, Stout HP. The friction of fibre assemblies. Wear 1960;3(1):26–42.
[5] Morrow JA. Frictional properties of cotton fibres. J Textile Inst Trans 1931;22:425.

[6] Martin AJP, Mittelmann R. Some measurements of the friction of wool and mohair. J Textile Inst Trans 1946;37(12):T269–80.
[7] Mercer EH, Makinson KR. The frictional properties of wool and other textile fibres. J Textile Inst Trans 1947;38(5):T227–40.
[8] Rubenstein C. Review on the factors influencing the friction of fibres, yarns and fabrics. Wear 1959;2(4):296–310.
[9] Howell HG, Mieszkis KW, Tabor D. Friction in textiles. London: Butterworths Scientific Publications; 1959.
[10] Yuksekkaya ME. More about fibre friction and its measurements. Textile Prog 2009;41(3):141–93.
[11] Amontons, G., 1699. De la résistance causée dans les machines. Mémoires de l'Académie Royale A, 257–282.
[12] Howell HG. Inter-fibre friction. J Textile Inst Trans 1951;42(12):T521–33.
[13] Tabor D. Friction, lubrication and wear of synthetic fibres. Wear 1957;1 (1):5–24.
[14] Roselman IC, Tabor D. The friction of carbon fibres. J Phys D Appl Phys 1976;9 (17):2517.
[15] Roselman IC, Tabor D. The friction and wear of individual carbon fibres. J Phys D Appl Phys 1977;10(8):1181.
[16] Bandyopadhyay SB. Frictional properties of jute and some other long vegetable fibers, Part I: general study of characters. Text Res J 1951;21:659–70.
[17] Bowden FP, Tabor D. The friction and lubrication of solids. Oxford: Clarendon Press; 1950.
[18] Archard JF. Elastic deformation and the laws of friction. Proc R Soc London Ser A, Math Phys Sci, 243(1233). p. 190–205.
[19] Greenwood JA, Williamson JBP. Contact of nominally flat surfaces. Proc R Soc London Ser A, Math Phys Sci, 295(1442). p. 300–19.
[20] Barber JR. Multiscale surfaces and Amontons' law of friction. Tribol Lett 2013;49(3):539–43.
[21] Mulvihill DM, Kartal ME, Nowell D, Hills DA. An elastic–plastic asperity interaction model for sliding friction. Tribol Int 2011;44(12):1679–94.
[22] Mulvihill DM, Sutcliffe MPF. Effect of tool surface topography on friction with carbon fibre tows for composite fabric forming. Compos Part A: Appl Sci Manuf 2017 [in press].
[23] Cornelissen B, de Rooij MB, Rietman B, Akkerman R. Frictional behaviour of high performance fibrous tows: a contact mechanics model of tow–metal friction. Wear 2013;305(1–2):78–88.
[24] Cornelissen B, Rietman B, Akkerman R. Frictional behaviour of high performance fibrous tows: friction experiments. Compos A Appl Sci Manuf 2013;44:95–104.
[25] Cornelissen B, de Rooij MB, Rietman B, Akkerman R. Frictional behavior of carbon fiber tows: a contact mechanics model of tow–tow friction. Text Res J 2014;84(14):1476–88.
[26] Chakladar ND, Mandal P, Potluri P. Effects of inter-tow angle and tow size on carbon fibre friction. Compos A Appl Sci Manuf 2014;65:115–24.
[27] Smerdova O, Sutcliffe MPF. Novel experimental method for microscale contact analysis in composite fabric forming. Exp Mech 2015;55(8):1475–83.
[28] Smerdova O, Sutcliffe MPF. Multiscale tool–fabric contact observation and analysis for composite fabric forming. Compos A Appl Sci Manuf 2015;73:116–24.
[29] Torayca T700S datasheet. Technical datasheet No. CFA-005. Torayca Carbon Fibers Inc, Santa Ana, CA, USA <http://www.toraycfa.com/pdfs/T700SDataSheet.pdf>.
[30] Chen B, Cheng AHD, Chou TW. A nonlinear compaction model for fibrous preforms. Compos A Appl Sci Manuf 2001;32(5):701–7.
[31] Mounier D, Poilâne C, Bûcher C, Picart P. Evaluation of transverse elastic properties of fibers used in composite materials by laser resonant ultrasound spectroscopy. Nantes, France: Société Française d'Acoustique. Acoustics 2012; 2012.
[32] Edupack CES. Cambridge UK: Granta Design Ltd; 2014.

Please cite this article in press as: Mulvihill DM et al. Friction of carbon fibre tows. Composites: Part A (2016), http://dx.doi.org/10.1016/j.compositesa.2016.08.034